Kovove Mater. 59 2021 69–78
DOI: 10.4149/km_2021_1_69

The influence of microstructure on hydrogen diffusion and embrittlement of fine-grained high strength dual-phase steels

A. Begić Hadžipašić[1]*, J. Malina[2], M. Malina[2]

[1] *University of Zagreb, Faculty of Metallurgy, Aleja narodnih heroja 3, 44000 Sisak, Croatia*
[2] *Stipe Kerepa 11, 44000 Sisak, Croatia*

Received 24 November 2011, received in revised form 12 February 2021, accepted 15 February 2021

Abstract

The permeation experiments performed in this study have shown that electrochemical corrosion of dual-phase steels in 2 mol L^{-1} H_2SO_4 results in hydrogen evolution and absorption of hydrogen atoms in the material, which leads to degradation known as hydrogen embrittlement (HE).

The values of the diffusion coefficient and hydrogen solubility obtained in this study have shown that transport of diffusible hydrogen and high susceptibility to HE depends on different microconstituents acting as hydrogen traps in dual-phase steels. The metallographic and SEM/EDS analyses have revealed elongated inclusions in dual-phase steel marked as DP, acting as irreversible traps in the ferrite-martensite matrix. Room temperature tensile tests of hydrogenated specimens have shown degradation of elongation and contraction compared to those of nonhydrogenated ones. SEM analyses of fracture surfaces have revealed the difference between nonhydrogenated dual-phase steels with ductile fracture and hydrogenated dual-phase steels with brittle fracture.

K e y w o r d s: dual-phase steel, hydrogen diffusion, hydrogen embrittlement, hydrogen traps, microstructure, mechanical properties

1. Introduction

The corrosion of steel in acid solution results besides iron dissolution also in the evolution of atomic hydrogen, which is an undesirable element in metals and their alloys [1, 2]. Except that hydrogen can subsequently be absorbed from the environment, it can be found in the metal crystal lattice as residual during production, processing or welding of steel [3, 4]. Since the only atomic form of hydrogen is able to move through the metal according to the laws of diffusion, because of its small atomic radius, it is called "diffusible" hydrogen. Once inside the material, hydrogen can diffuse or be trapped by the different defects existing in the material, such as dislocations, grain boundaries, and non-metallic inclusions, leading to the weakening of bonds between different microconstituents and to the phenomenon of hydrogen embrittlement [5–7].

Hydrogen embrittlement is a specific type of stress corrosion cracking caused by hydrogen, often combined with applied and residual stress. The consequence of hydrogen embrittlement is the deterioration of mechanical properties of structural steel and decrease of bearing capacity of component followed by sudden fracture of construction [3, 8]. Generally, a small quantity of hydrogen is sufficient to cause failures because it can magnify its effect by migrating to high triaxial stress regions. The problem of hydrogen embrittlement in structural alloys has been of great concern in various industries, including power plants. Hydrogen embrittlement or hydriding has led to the failures of fuel cladding in nuclear reactors, cracking of fossil fuel boiler tubes, and many other components where there is a possibility of hydrogen ingress in the material [9].

However, as the demands of the automotive industry for greater strength and deformation ability are further increased, new families of high strength steel have been developed. These new steel grades include

*Corresponding author: tel.: + 385 44 533 379 (local 219); fax: + 385 44 533 378; e-mail address: begic@simet.unizg.hr

DP (dual phase), TRIP (transformation induced plasticity), FB (ferrite-bainite), CP (complex phase), and TWIP (twinning induced plasticity) steels [10–12]. Unlike the conventional high strength steels, where increasing strength simultaneously with increasing plasticity is obtained by conventional thermal treatment, "modern" high strength steels achieve that by thermomechanically controlled process (TMCP) and microalloying [3, 8, 13]. The characteristic of such TMCP steel is multiphase fine-grained microstructure with great ability of high impact energy ("stretch effect"). These modern high strength steels have application in the automotive industry, for bridge constructions, for production of pressure vessels, high-pressure line-pipes, etc. [14, 15]. Since their application in different exploitation conditions is not known enough, in this work, the influence of microstructure on hydrogen diffusion and embrittlement of dual-phase steels is studied by monitoring hydrogen permeation with electrochemical technique.

Hydrogen permeation through a metallic membrane by an electrochemical technique is a widely used method for studying hydrogen diffusivity and metallic embrittlement phenomenon [6, 16–18]. In the course of electrochemical permeation, hydrogen atoms are first absorbed in the entry surface, then diffused through the metallic membrane, and are finally desorbed from the exit surface. On the entry surface, hydrogen production can be controlled galvanostatically or potentiostatically or under the metal's free corrosion status. On the exit surface, it is usual to apply a constant potential to ensure that all hydrogen atoms can be ionized, assuring that the measured current density is the hydrogen permeation flux.

2. Experimental

The samples were prepared from the low-carbon high strength hot-rolled strips of dual-phase steels of different chemical composition marked as DP and A (Table 1).

It can be seen from Table 1 that dual-phase steels have low sulphur and phosphor content, which provides high purity and quality of examined steels because it minimizes the possibility of sulphides formation and other inclusions.

To investigate the tendency to hydrogen embrittlement, it is necessary to hydrogenate the samples. The penetration of hydrogen atoms through the steel materials can be accelerated by a simple laboratory procedure of electrochemical examination of hydrogen diffusion in ferrous materials [19]. For permeation experiments, the samples of dual-phase steels marked as DP and A were cut from steel sheets of original thickness into the membranes with the following dimensions: $(50 \times 80 \times 1.5)\,\mathrm{mm}^3$ for DP, $(50 \times 80 \times 1.65)\,\mathrm{mm}^3$ for A. Anodic (exit) side of samples was coated with nickel so that the surface at the oxidation side of the metallic membrane is passive or corrosion resistant. Before every measurement, the entry side of the membrane was ground with emery paper to a 600 grit finish. After that, the membrane was rinsed in distilled water and degreased in ethanol.

Table 1. Chemical composition of examined dual-phase steels (mass %)

Sample	DP	A
C	0.05	0.073
Mn	1.23	1.85
Si	0.42	0.013
P	0.012	0.015
S	0.003	0.004
Al	0.033	0.047
N	0.0085	0.0060
Cu	0.16	0.014
Nb	0.002	0.002
Ti	–	0.001
Mo	0.01	–
V	–	0.003
Cr	0.66	0.221
Ni	0.05	–
Sn	0.008	–

The experimental device for monitoring hydrogen diffusion through metallic membrane consists of the cell for hydrogen charging (entry part-filled with 2M H_2SO_4 deaerated with nitrogen) and oxidation cell (exit part-filled with 1M NaOH), which are separated by a thin steel plate (sample-working electrode, whose entry side is placed in contact with charging cell) [13, 19]. Saturated calomel electrode (SCE) as reference electrode and Pt-plate as counter electrode are placed in oxidation cell, so that the potential of steel membrane is maintained in the passivity area: +200 mV *vs* SCE by "PARSTAT" Potentiostat/Galvanostat (Princeton Applied Research, USA) Model 2273. In the charging cell, the hydrogen evolution occurs through the corrosion reaction of steel with H_2SO_4. In the oxidation cell (exit part), no captured hydrogen at the exit side of the membrane oxidizes in H^+-ions by the influence of applied potential. The current flow between the steel membrane and counter electrode is registered as permeation current I (μA), which presents the measure for the amount of hydrogen diffuses through the steel membrane.

Because the samples for permeation experiments were not of the same thickness, the given values are reduced to normalized values and displayed graphically in the form of the normalized flux of atomic hydrogen $J(t)/J_{\mathrm{ss}}$ against the normalized time τ [20]. Based on such a presentation, mathematical modelling of hydrogen diffusion could be performed. The mathematical models for the study of permeation transient through

the metallic membrane were developed for potentiostatic and galvanostatic charging based on Fick's laws. Two models were used for mathematical modelling of hydrogen diffusion to find out which model fits experimental diffusion curves of examined materials [17]:

– CC model of constant concentration, Eq. (1):

$$\frac{I_\mathrm{t}}{I_\infty} = \frac{2}{(\pi\tau)^{1/2}} \sum_{n=0}^{\infty} \exp\left[-\frac{(2n+1)^2}{4\tau}\right], \qquad (1)$$

– CF model of constant flux, Eq. (2):

$$\frac{I_\mathrm{t}}{I_\infty} = 1 - \frac{4}{\pi} \sum_{n=0}^{\infty} \frac{(-1)^n}{(2n+1)} \exp\left[-\frac{(2n+1)^2\pi^2\tau}{4}\right], \qquad (2)$$

where I_t is the permeation current at instant time t, and I_∞ is the steady-state value of the hydrogen permeation current. The dimensionless time τ is equal to Dt/L^2, where D is the hydrogen diffusion coefficient, and L is the membrane thickness.

A degradation of investigated dual-phase steels caused by hydrogen absorption through corrosion reaction could be evaluated based on changes in mechanical properties of hydrogenated samples. For this purpose, specimens for tensile testing were cut in the rolling direction and ground with emery paper to a 600 grit finish [21]. After that, the samples were rinsed in distilled water, degreased in ethanol and immersed in 2 M H_2SO_4. In the charging cell, saturated calomel electrode as reference electrode and Pt-net as counter electrode were placed next to the working electrode. To accelerate the charging of specimens, cathodic polarization was carried out for four hours at a potential of –700 mV *vs* SCE by "PARSTAT" Potentiostat/Galvanostat Model 2273. After cathodic polarization, the specimens were tensile tested at a crosshead speed of 2 mm min^{-1}and room temperature using a universal testing machine Instron. The dimensions of the tensile testing samples comply with the standard EN 10002-1: 1990 [21]. So, width of the samples for tensile tests was 20 mm, thickness 3 mm, test length 120 mm, while the total length of the tensile testing samples (together with the heads entering the universal testing machine) was 250 mm. The ultimate tensile strength was determined by the maximum force ratio applied during the tensile test to the cross-sectional area of the tested part of the sample.

Four samples of DP and four samples of A dual-phase steel were prepared; two of each dual-phase steels were tensile tested before and after hydrogenation. As a result, the arithmetic values of the two measurements obtained for each type of dual-phase steel before and after hydrogenation were taken.

For metallographic investigations and microstructural characterization, the samples were cut in the rolling direction and pressed by "SimpliMet®" machine for hot pressing of samples. After that, the samples were ground (emery paper No. 400, 500, 600, and 800 grit) and polished by the "Buehler" automatic device. Thus prepared samples were observed by optical microscope with "Olympus GX 51" digital camera with a system for automated picture analysis (AnalySIS® Materials Research Lab) to detect the inclusions. After that, the samples were etched by Nital (5 % HNO_3 in ethanol) to record their microstructure.

SEM/EDS analysis of sample microstructure, fracture surfaces and registered inclusions were carried out by scanning electron microscope "Tescan Vega LSH" (Czech Republic) equipped with "Bruker" EDS spectrometer.

3. Results and discussion

Based on hydrogen permeation electrochemical measurements and obtained diagrams $i = f(t)$, the steady-state permeation current density of atomic hydrogen i_ss and time t_lag (which presents a time to achieve a value of $0.63i_\mathrm{ss}$) were determined [20]. Also, the other diffusion parameters were calculated, such as diffusion coefficient D_eff, the amount of atomic hydrogen passing through the metal membrane per unit area in a steady-state condition $n(\mathrm{H_2})$, the volume of atomic hydrogen passing through the metal membrane per unit area in a steady-state condition $V(\mathrm{H_2})$, atomic hydrogen permeation flux at steady-state J_ss and the sub-surface concentration of hydrogen in interstitial lattice sites and reversible trap sites on the charging side of the sample C_0R [20]. All diffusion parameters were calculated as the arithmetic mean of the second, third, and fourth permeation transient and presented in Table 2. The first permeation transient was omitted because all traps are filling at the first measurement, and we wanted to show only the influence and meaning of reversible traps. Namely, diffusible hydrogen trapped in reversible traps is dangerous because it can move through a crystal lattice for a long time until it finds a suitable place. It can also move from one place to another and cause additional stress in a crystal lattice and, consequently, the delayed fracture [2, 4, 8, 9].

It can be seen from Table 2 that both dual-phase steels have diffusion coefficient three orders of magnitude lower than that in the crystal lattice of α-Fe ($D_\mathrm{Fe} = 1.28 \times 10^{-4}\,\mathrm{cm^2\,s^{-1}}$) [16]. It means that traps are present, which slow down the transport of H-atoms through a membrane. It is important to notice that dual-phase steel marked as A showed lower D_eff and higher C_0R than that in dual-phase steel marked as DP, which indicates that dual-phase steel A has more reversible traps. However, the nature of traps present in the material and their bond strength are more im-

Table 2. Hydrogen diffusion parameters for examined dual-phase steels

Sample	DP	A
E_{corr} (mV) *vs* SCE	–240	–430
L (cm)	0.15	0.16
i_{ss}(μA cm^{-2})	3.19	1.90
t_{lag} (s)	5202	11612
$n(H_2) \times 10^6$ (mol cm^{-2})	0.15	0.20
$V(H_2) \times 10^3$ (cm^{3}H$_2$ cm^{-2})	3.29	4.36
$D_{eff} \times 10^7$ (cm^2 s^{-1})	7.21	3.93
$J_{ss} \times 10^{11}$ (mol cm^{-2} s^{-1})	3.31	1.97
$C_{0R} \times 10^6$ (mol H cm^{-3})	6.89	8.28

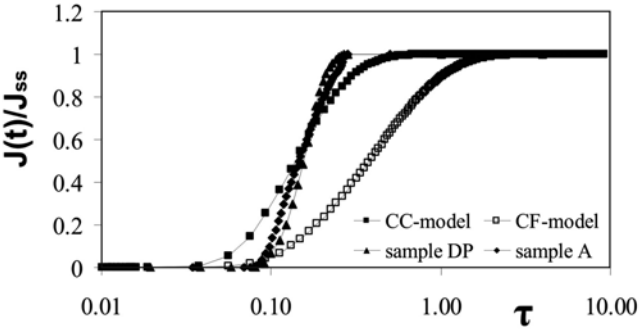

Fig. 1. Mathematical modelling of the normalized time dependence of the normalized flux of atomic hydrogen for investigated dual-phase steels.

portant than their quantity. Namely, it is known that decreasing of D_{eff} and increasing of C_{0R} strongly depends on hydrogen trapping. The most frequently appearing traps are different material defects such as dislocations, grain boundaries, inclusions, etc. [5, 6, 22–24]. In this work, only the amounts of diffused hydrogen on the other side of the sample membrane were measured, but not the amount of absorbed hydrogen. Recent research allows the determination of the concentration of absorbed hydrogen in the metal and also study the effects of deformation on the sample monitored by the DIC method (digital image correlation), which gives a broader picture of the influence of hydrogen on the diffusion and embrittlement of metals [25].

The mathematical modelling of hydrogen diffusion of examined dual-phase steels is shown in Fig. 1. For that purpose, the normalized flux of atomic hydrogen $J(t)/J_{ss}$ and normalized time τ were calculated [20].

Based on Fig. 1, it can be concluded that normalized curves of both samples are fitted more to the CC-model, which means that experimental curves of examined dual-phase steels are following initial and boundary conditions determined according to the model of constant concentration. Furthermore, Fig. 1 shows the steeper normalized curves for both samples, indicating the presence of irreversible traps to a minor extent (MnS-inclusions, carbides) [20].

Room temperature tensile tests of nonhydrogenated and hydrogenated samples of examined dual-phase steels indicate that elongation and contraction of these steels deteriorate after hydrogenation (Table 3), which means that hydrogen has an unfavourable effect on room temperature ductility. However, in the case of combined thermal and hydrogen embrittlement effects, the situation is much more complicated. There are plenty of different microstructural sites in steels, such as grain boundaries, free dislocations, precipitates, and inclusions that may interact with absorbed hydrogen and affect the resulting ten-

Table 3. Room temperature tensile properties of examined dual-phase steels before and after hydrogenation

Sample	Yield strength R_e (MPa)	Tensile strength R_m (MPa)	Elongation A (%)	Contraction Z (%)	Index of hydrogen embrittlement HE (%)
DP	Before hydrogenation				58.58
	545	628	24.0	63.5	
	After hydrogenation				
	468	628	20.0	26.3	
A	Before hydrogenation				35.75
	325	559	37.4	66.3	
	After hydrogenation				
	341	561	30.0	42.6	

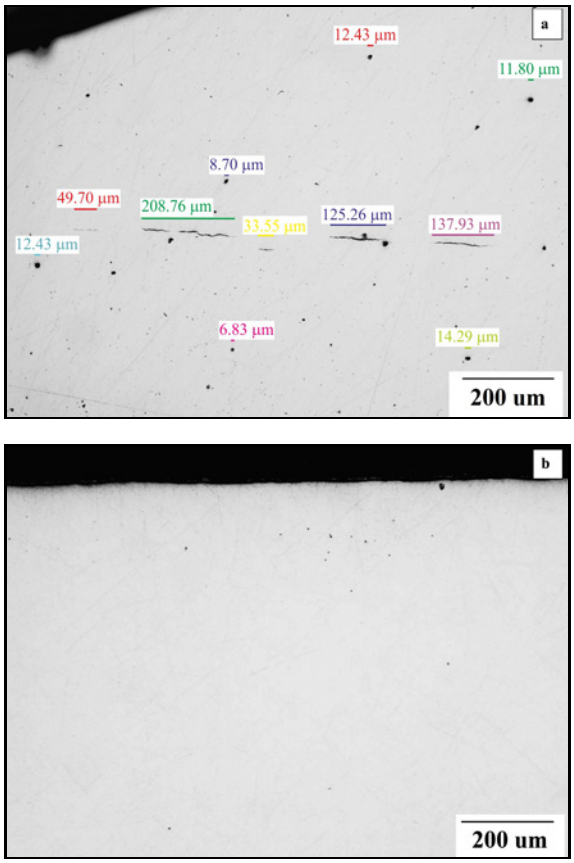

Fig. 2. Optical micrographs: (a) globular and elongated inclusions in dual-phase steel DP and (b) globular inclusions in dual-phase steel A.

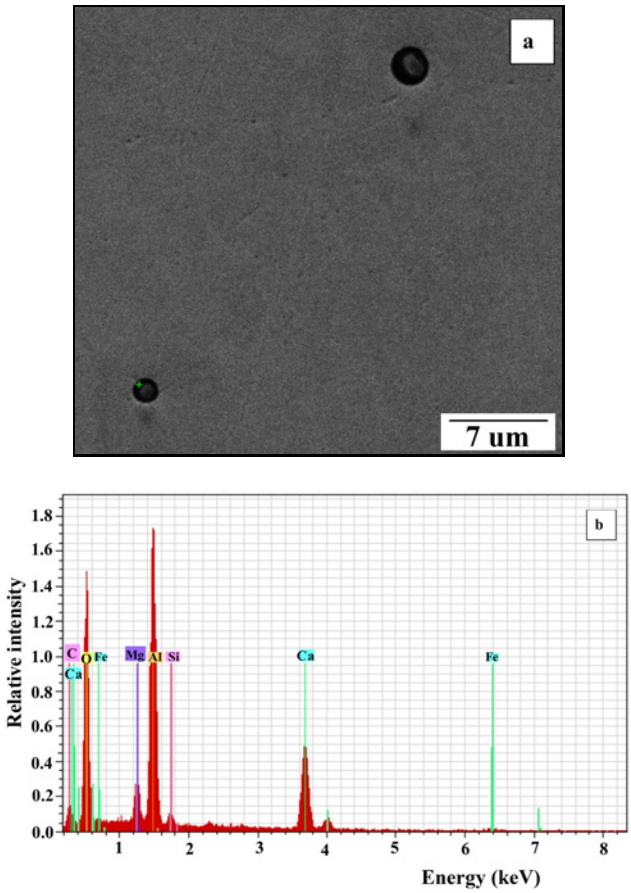

Fig. 3. (a) SEM micrograph of globular inclusion in dual-phase steel DP [13] and (b) EDS analysis of globular inclusion in dual-phase steel DP [13].

sile properties and fracture behaviour [26].

In this research, deterioration of mechanical properties in dual-phase steel marked as A has been registered to a minor extent which can be classified as more resistant material to hydrogen embrittlement than dual-phase steel DP. Namely, because of different strengthening concepts (based on manganese and carbon), less martensite was obtained in sample A, resulting in an increased elongation and contraction compared to those in the sample DP. Moreover, it has been shown that the elongation of sample A was higher after hydrogenation than that of the sample DP before hydrogenation. The index of hydrogen embrittlement *HE* has also been shown in Table 3 as the indicator of hydrogen embrittlement, which was calculated according to the following equation [15], Eq. (3):

$$HE = \frac{Z(\text{air}) - Z(H_{\text{abs}})}{Z(\text{air})} \times 100, (\%) \qquad (3)$$

where $Z(\text{air})$ is the contraction of the nonhydrogenated sample, and $Z(H_{\text{abs}})$ is the contraction of the hydrogenated sample.

The sample of dual-phase steel marked as A showed a lower *HE* index than that in the sample DP, which means that sample A has better resistance to hydrogen embrittlement.

Since irreversible traps can be various carbides and inclusions (especially MnS), they are significantly presented in examined dual-phase steel marked as DP. Namely, metallographic and SEM analyses of dual-phase steel DP revealed many globular inclusions dimensions from 2–10 µm and some elongated inclusions dimensions from 20–100 µm (Figs. 2a, 3a, 4a).

EDS analysis of globular inclusion in the sample DP revealed the presence of (Ca, Al)-oxides because it has been registered an increasing content of oxygen, calcium, and aluminium (Fig. 3b). The formation of these complex oxides is caused by calcium treatment in ladle furnace, leading to increasing their hardness and keeping their globular shape through forming process [8, 11, 13]. In contrast to that, the elongated MnS inclusions with bigger dimensions increase anisotropic properties and the number of irreversible traps. The EDS analysis of elongated inclusions in the sample DP has shown an increased content of oxygen, aluminium, manganese, carbon, and sulphur (Fig. 4b), which indicates the fact that (Al, Mn)-oxisulphides and (Al,

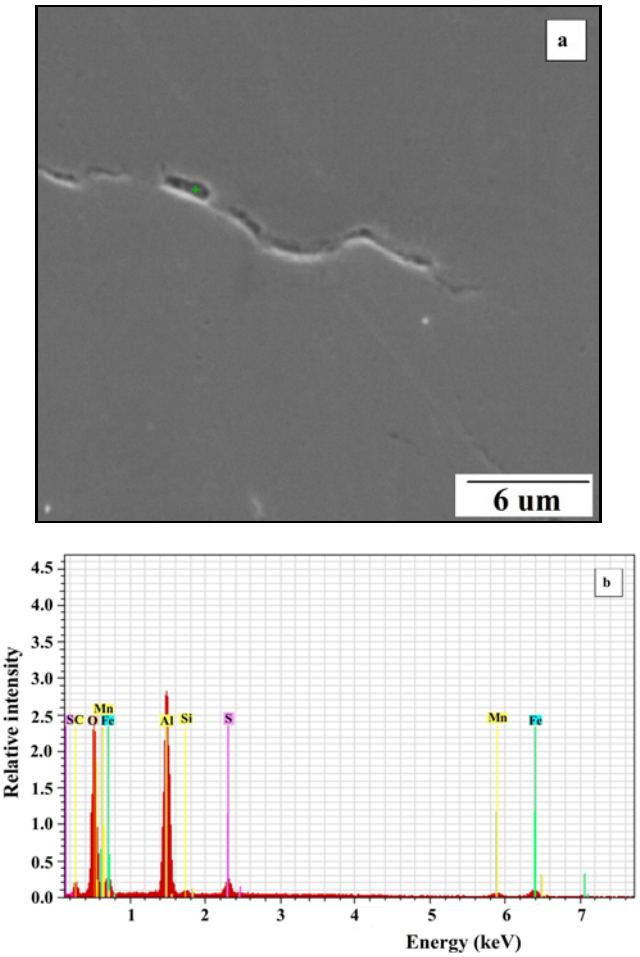

Fig. 4. (a) SEM micrograph of elongated inclusion in dual-phase steel DP [13] and (b) EDS analysis of elongated inclusion in dual-phase steel DP [13].

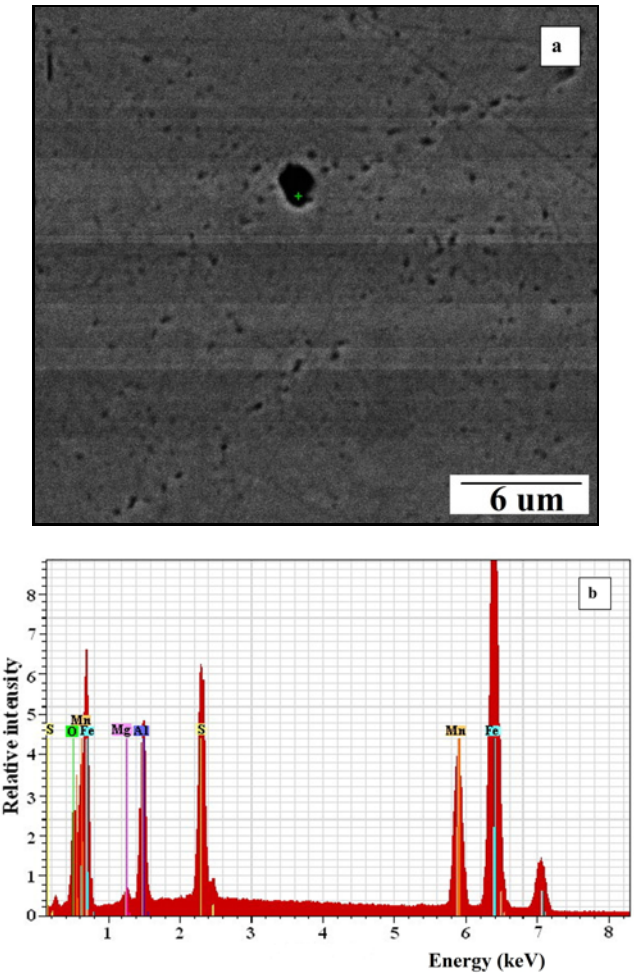

Fig. 5. a) SEM micrograph of globular inclusion in dual-phase steel A and (b) EDS analysis of globular inclusion in dual-phase steel A.

Mn)-oxicarbides are present in the studied sample.

There were not registered any elongated inclusions in the sample of dual-phase steel marked as A. Still, some globular inclusions dimensions from 2–7 μm (Fig. 2b) indicate that the presence of irreversible traps is decreased in this type of dual-phase steel. The SEM/EDS analysis of globular inclusion in dual-phase steel A confirmed the presence of (Mn, Al)-oxisulfides because of the increased content of manganese, oxygen, sulphur, and aluminium (Fig. 5).

In contrast to that, the reversible traps are represented as dislocations and grain boundaries, especially between two phases, which can be concluded by analysing the microstructures of examined dual-phase steels (Fig. 6). In addition to research obtained on dual-phase steels, previously conducted research on IF steels has shown that various inclusions and impurities have proven to be ideal irreversible hydrogen traps [27]. It has also been found that performing permeation one after the other leads to shortening of the hydrogen passage time to the other side of the membrane because only reversible traps slow down hydrogen transport [27].

Optical and SEM micrographs of the microstructure of studied samples etched by Nital show that both steels have an extremely fine-grained microstructure which consists of ferrite matrix and islands of martensite. Since the microstructure is fine-grained, the high density of dislocations and numerous grain boundaries provide more extended travel of atomic hydrogen through a crystal lattice of examined materials and, therefore, slower breakdown of hydrogen at the opposite side of the membrane. It is essential to notice that dual-phase steel DP has a microstructure with a larger amount of martensite because of different strengthening mechanism concerning the sample A. Namely, sample A has in its chemical composition an increased content of manganese and carbon while strengthening mechanism in the sample DP is accomplished by increasing the content of manganese, silicon, and chromium. Typically, chromium is known as an austenite stabilizer, and it decreases the cool-

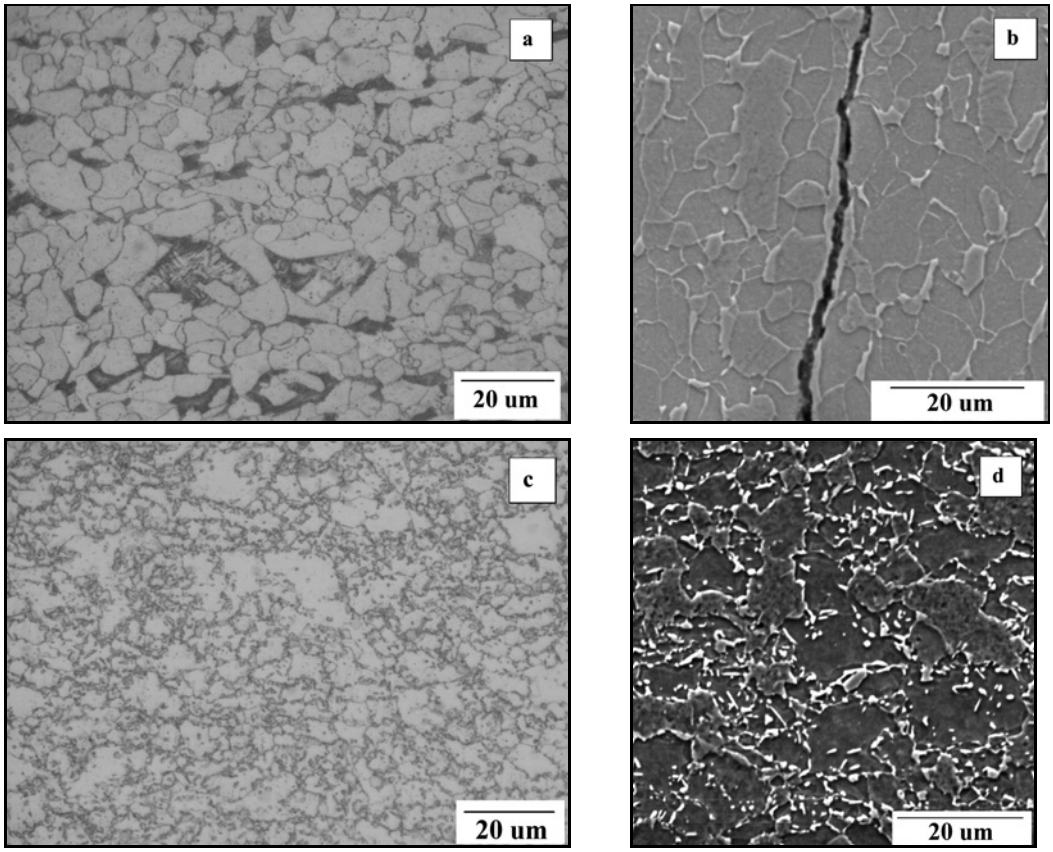

Fig. 6. (a) Optical micrograph of dual-phase steel DP etched by Nital, (b) SEM micrograph of dual-phase steel DP etched by Nital, (c) optical micrograph of dual-phase steel A etched by Nital, and (d) SEM micrograph of dual-phase steel A etched by Nital.

ing rate needed for transformation without diffusion [4, 28]. That helps the formation of martensite, which is the unfavourable phase in microstructure from the hydrogen embrittlement aspect because of its lower solubility of carbon and hydrogen and higher hardness.

The SEM analysis also revealed that elongated inclusions in the sample DP were mostly found in the centre of the sample DP and in the rolling direction because the segregation of all impurities occurs in the centre of the hot-rolled strip. Also, the propagation of elongated inclusions at grain boundaries was determined because grain boundaries are favourable places for accumulating different segregations, which form inclusions during rolling (Fig. 6b).

The SEM analysis of fracture surfaces of hydrogenated dual-phase steels again confirms that hydrogen has a detrimental effect on material properties (Fig. 7). Namely, the nonhydrogenated samples of dual-phase steels showed a ductile fracture, while hydrogenated samples showed cleavage transgranular fracture. Furthermore, it has been noticed at the sample DP that hydrogen was mostly accumulated in the impurities of the segregation zone, which caused the increase of pressure and evolution of crack along with the whole sample in the rolling direction (Figs. 7b, c). Such a phenomenon was not registered in sample A.

Considering the obtained results, it can be concluded that dual-phase steel A showed better resistance to hydrogen embrittlement compared to that of DP because of its different strengthening concept, the less martensite, fewer inclusions, better elongation, and lower *HE* index.

4. Conclusions

Based on the given results obtained in this work by electrochemical, mechanical, metallographic, and SEM/EDS examinations, the influence of microstructure on hydrogen diffusion and embrittlement of fine-grained high strength dual-phase steels was studied.

The conducted experiments have provided the following conclusions:

– The diffusion coefficients three orders of magnitude lower than that in the crystal lattice of α-Fe were obtained, which means that traps are present and slow down the transport of H-atoms through a membrane of both dual-phase steels during permeation experiments.

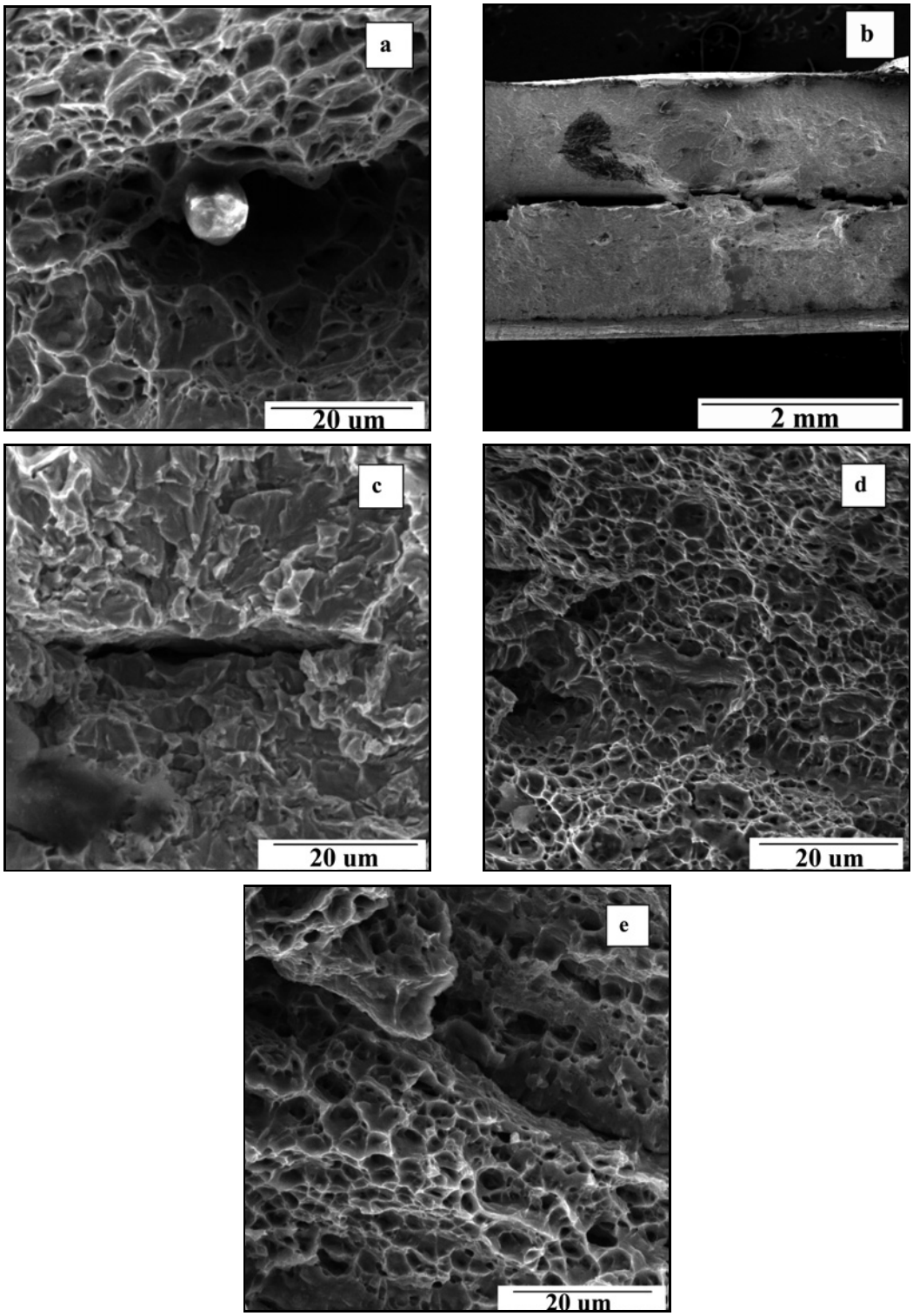

Fig. 7. SEM micrographs of fracture surfaces of examined dual-phase steels: (a) DP before hydrogenation, (b) DP after hydrogenation, (c) DP after hydrogenation, (d) A before hydrogenation, and (e) A after hydrogenation.

– The mathematical modelling of permeation curves of examined dual-phase steels showed that normalized curves of both samples are fitted more to the CC-model, which means that experimental curves of examined steel materials are following initial and boundary conditions determined according to the model of constant concentration. Furthermore, the steeper normalized curves for both samples indicate that less irreversible traps (MnS-inclusions, carbides) are present.

– Optical and SEM micrographs of the microstructure of examined samples show that both steels have an extremely fine-grained microstructure which consists of ferrite matrix and islands of martensite.

– The elongation and contraction of examined dual-phase steels deteriorate after hydrogenation, which means that hydrogen has an unfavourable effect on room temperature tensile properties of examined steel materials.

– Metallographic and SEM/EDS analysis of dual-phase steel DP revealed a significant number of (Ca, Al)-oxides as globular inclusions and some (Al, Mn)-oxisulphides and (Al, Mn)-oxicarbides as elongated inclusions. In contrast to that, in dual-phase steel A, only the presence of globular inclusions type (Mn, Al)-oxisulfide was registered, indicating the presence of irreversible traps decreased in this type of dual-phase steel.

– The SEM analysis of nonhydrogenated samples of dual-phase steels showed a ductile fracture, while hydrogenated samples showed cleavage transgranular fracture. Also, hydrogen in the sample DP was mostly accumulated in the impurities in the segregation zone, which caused the increase of pressure and evolution of crack along with the whole sample in the rolling direction.

– The better resistance to hydrogen embrittlement of sample A compared to that of the sample DP can be assigned to its different strengthening concept due to less martensite, fewer inclusions, lower HE index, and better elongation and contraction.

Acknowledgement

This work was supported by the Ministry of Science, Education and Sport of the Republic of Croatia within the project 124-1241565-1524.

References

[1] H. J. Grabke, E. Riecke, Absorption and diffusion of hydrogen in steels, Mater. Tehnol. 34 (2000) 331–342.
[2] A. M. Brass, J. Chene, Hydrogen uptake in 316L stainless steel: Consequences on the tensile properties, Corros. Sci. 48 (2006) 3222–3242. doi:10.1016/j.corsci.2005.11.004
[3] J. Malina, G. Vručinić, M. Malina, Evaluation of welded TMCP steel for resistance to HIC and SSC, Weld. World 51 (2007) 537–546.
[4] B. Beidokhti, A. Dolati, A. H. Koukabi, Effects of alloying elements and microstructure on the susceptibility of the welded HSLA steel to hydrogen-induced cracking and sulfide stress cracking, Mater. Sci. Eng. A 507 (2009) 167–173. doi:10.1016/j.msea.2008.11.064
[5] A. M. Brass, F. Guillon, S. Vivet, Quantification of hydrogen diffusion and trapping in 2.25Cr-1Mo and 3Cr-1Mo-V steels with the electrochemical permeation technique and melt extractions, Metall. Mater. Trans. A 35A (2004) 1449–1464. doi:10.1007/s11661-004-0253-y
[6] T. Zakroczymski, Adaptation of the electrochemical permeation technique for studying entry, transport and trapping of hydrogen in metals, Electrochim. Acta 51 (2006) 2261–2266. doi:10.1016/j.electacta.2005.02.151
[7] S. Serna, H. Martinez, S. Y. López, J. G. Gonzáles-Rodrígues, J. L. Albarrán, Electrochemical technique applied to evaluate the hydrogen permeability in microalloyed steels, Int. J. Hydrog. Energy 30 (2005) 1333–1338. doi:10.1016/j.ijhydene.2005.04.012
[8] J. Malina, I. Samardžić, V. Gliha, Susceptibility to hydrogen-induced cracking of weld beads on high-strength structural steel, Mater. Sci. 41 (2005) 253–258. doi:10.1007/s11003-005-0158-y
[9] R. K. Dayal, N. Parvathavarthini, Hydrogen embrittlement in power plant steels, Sadhana 28 (2003) 431–451. doi:10.1007/BF02706442
[10] J. Zrnik, I. Mamuzić, S. V. Dobatkin, Recent progress in high strength low carbon steels, Metalurgija 45 (2006) 323–331.
[11] K. E. Hensger, Processing of advanced structural steels on CSP plants, Metalurgija 41 (2002) 183–190.
[12] L. Zhuang, W. Di, H. Rong, Austempering of hot rolled Si-Mn TRIP steels, J. Iron. Steel Res. Int. 13 (2006) 41–46. doi:10.1016/S1006-706X(06)60093-9
[13] A. Begić Hadžipašić, J. Malina, M. Malina, The influence of microstructure on hydrogen diffusion and embrittlement of multiphase fine-grained steels with increased plasticity and strength, Chem. Biochem. Eng. Q. 25 (2011) 159–169.
[14] S. Dey, A. K. Mandhyan, S. K. Sondhi, I. Chattoraj, Hydrogen entry into pipeline steel under freely corroding conditions in two corroding media, Corros. Sci. 48 (2006) 2676–2688. doi:10.1016/j.corsci.2005.10.003
[15] M. Mihaliková, M. Német, The hardness HV1 analysis of automotive steels sheets after the plastic deformation, Acta Metall. Slovaca 17 (2011) 26–31.
[16] U. Hadam, T. Zakroczymski, Absorption of hydrogen in tensile strained iron and high-carbon steel studied by electrochemical permeation and desorption techniques, Int. J. Hydrog. Energy 34 (2009) 2449–2459. doi:10.1016/j.ijhydene.2008.12.088
[17] Y. F. Cheng, Analysis of electrochemical hydrogen permeation through X-65 pipeline steel and its implications on pipeline stress corrosion cracking, Int. J. Hydrog. Energy 32 (2007) 1269–1276. doi:10.1016/j.ijhydene.2006.07.018
[18] J. Sojka, F. Filuš, L. Rytířová, M. Jerome, Diffusion characteristics of hydrogen in micro alloy steels, Acta Metall. Slovaca 13 (2007) 554–560.
[19] M. A. V. Devanathan, Z. Stachurski, The mechanism of hydrogen evolution on iron in acid solutions by determination of permeation rates, J. Electrochem. Soc. 111 (1964) 619–623. doi:10.1149/1.2426195
[20] EN ISO 17081:2008, Method of measurement of hydrogen permeation and determination of hydrogen uptake and transport in metals by an electrochemical technique.
[21] EN 10002-1:1990, Metallic materials-tensile testing – Part 1: Method of test at ambient temperature.
[22] Š. Nižnik, M. Zavacký, G. Janák, Ľ. Furman, New possibility of hydrogen traps formation in deep drawing

IF steel sheets for enameling, Acta Metall. Slovaca 13 (2007) 336–344.
[23] A. Begić Hadžipašić, J. Malina, Š. Nižnik, The influence of microstructure on hydrogen diffusion in dual phase steel, Acta Metall. Slovaca 17 (2011) 129–137.
[24] J. Blach, P. Zahumensky, Fracture manifestations of low-alloyed 2.6CrMoV steels under tensile test conditions in subtransition temperature range, Kovove Mater. 34 (1996) 143–156.
[25] M. Stamborska, J. Lapin, O. Bajana, Effect of hydrogenation on deformation behaviour of ferritic-pearlitic steel studied by digital image correlation method, Kovove Mater. 54 (2016) 397–406. doi:10.4149/km_2016_6_397
[26] L. Falat, L. Čiripová, V. Homolová, P. Futáš, P. Ševc, Hydrogen pre-charging effects on the notch tensile properties and fracture behaviour of heat-affected zones of thermally aged welds between T24 and T92 creep-resistant steels, Kovove Mater. 54 (2016) 417–427. doi:10.4149/km_2016_6_417
[27] A. Begić Hadžipašić, J. Malina, Š. Nižnik, Influence of microstructure on hydrogen diffusion and impedance of IF steel, Kovove Mater. 50 (2012) 345–350. doi:10.4149/km_2012_5_345
[28] S. K. Albert, V. Ramasubbu, N. Parvathavarthini, T. P. S. Gill, Influence of alloying on hydrogen-assisted cracking and diffusible hydrogen content in Cr-Mo steel welds, Sadhana 28 (2003) 383–393. doi:10.1007/BF02706439